JOURNAL OF APPLIED PHYSICS **115**, 183903 (2014)

Magneto-optical Kerr effect in $L1_0$ FePdPt ternary alloys: Experiments and first-principles calculations

L. Ma,[1] J. Hu,[2] M. Costa,[2] Z. Shi,[1] J. Li,[3] X. G. Xu,[4] Y. Jiang,[4] G. Y. Guo,[5,6] R. Q. Wu,[2,a)] and S. M. Zhou[1,a)]

[1]*Shanghai Key Laboratory of Special Artificial Microstructure and Pohl Institute of Solid State Physics and School of Physics Science and Engineering, Tongji University, Shanghai 200092, China*
[2]*Department of Physics and Astronomy, University of California, Irvine, California 92697-4575, USA*
[3]*School of Optics Science and Engineering, Fudan University, Shanghai 200433, China*
[4]*State Key Laboratory for Advanced Metals and Materials, School of Materials Science and Engineering, University of Science and Technology Beijing, Beijing 100083, China*
[5]*Department of Physics, National Taiwan University, Taipei 106, Taiwan*
[6]*Graduate Institute of Applied Physics, National Chengchi University, Taipei 116, Taiwan*

(Received 28 March 2014; accepted 13 April 2014; published online 13 May 2014)

We have studied the magneto-optical Kerr effect (MOKE) of $L1_0$ $Fe_{0.5}(Pd_{1-x}Pt_x)_{0.5}$ alloy films with both experiments and first-principles calculations. In the visible region, negative Kerr rotation and ellipticity peaks are, respectively, observed in the regions of 1.5–2.0 eV and 1.7–2.6 eV. These peaks are shifted towards higher energies, and their magnitudes are enhanced for larger x. The MOKE evolution is mainly ascribed to the anomalous Hall conductivity contributed by the spin-down $d_{\downarrow,x^2-y^2}$ bands from Pd and Pt. We established a close correlation among the MOKE spectra, the spin orbit coupling strength, and the band feature for this prototypical system. © *2014 AIP Publishing LLC*. [http://dx.doi.org/10.1063/1.4872463]

INTRODUCTION

As one of the most important properties of magnetic materials, magneto-optical Kerr effect (MOKE) arises from the interplay between the exchange splitting and the spin orbit coupling (SOC). The MOKE has been generally believed to scale linearly with the spontaneous magnetization and has become a high sensitivity tool to probe the magnetization behavior of magnetic films, in particular magnetic ultrathin films.[1–4] The spectroscopic features of the Kerr rotation θ_K and Kerr ellipticity ε_K can be assigned to specific interband transitions, so the MOKE spectra have also been widely employed to study the energy band structures.[5–12] Remarkably, the close correlation between the MOKE and magnetocrystalline anisotropy has been known for years due to the same physical origins of the SOC.[13,14] However, there have been very few reports about the dependence of the MOKE on the SOC strength.[15] The exact correlation between MOKE signal, energy band structure, and more intrinsically the SOC strength hence remains mysterious, although it has been extensively studied.[16–20] This inspires us to study the MOKE spectra of structurally ordered alloys, in which the SOC strength and energy band structure can be *artificially* controlled.

$L1_0$ $Fe_{0.5}(Pd_{1-x}Pt_x)_{0.5}$ (=FePdPt) alloy films are *exclusively ideal* objects to address above issues, i.e., the qualitative dependence of the MOKE on both the SOC strength and the energy band structure. The energy band structure and in particular the effective SOC strength of the FePdPt alloys change with x in a simple way because Pd and Pt atoms have different atomic order numbers. For the $L1_0$ FePt and FePd alloys, the enhanced θ_K near $E = 2.0$ eV and 4.5 eV is experimentally observed, in comparison with those of disordered FePt and FePd alloys.[21,22] The θ_K of $L1_0$ FePt films is larger than that of $L1_0$ FePd films, which was attributed to the stronger spin orbit coupling of heavier Pt atoms. Moreover, it was recognized that the θ_K peak of $L1_0$ FePt locates at the high energy side, compared with that of $L1_0$ FePd films,[10,12,21,22] indicating the effects of the energy band structures on the MOKE spectra. It is noted that the FePdPt alloys are important media in high density recording and their magnetic properties have been extensively explored in the past decades.

In this work, we study the *evolution* of the MOKE spectra of epitaxial $L1_0$ FePdPt alloy films with the Pt/Pd atomic concentration, x. Through both density functional calculations and experimental measurements, the SOC tuning effect is clearly demonstrated on the MOKE spectra. For all $L1_0$ FePdPt alloys, the measured θ_K spectra display a negative peak and a dip in the visible region. When the concentration of Pt increases, the peak and the dip shift toward higher energies, along with gradual enhancement in magnitude. First-principles calculations show that the MOKE feature can be attributed to change of the $d_{\downarrow,x^2-y^2}$ band of the Pt/Pd with x, where the arrow indicates the minority spin channel. Our results provide clear understanding of both the mechanism of the MOKE and electronic properties of the $L1_0$ ordered magnetic alloys.

EXPERIMENTS

A series of $L1_0$ FePdPt films were deposited by DC magnetron sputtering on MgO(002) substrates in an ultrahigh vacuum system with the Pt(002) buffer layer. The base pressure and Ar pressure during deposition were 1.0×10^{-5} Pa and

a)Authors to whom correspondence should be addressed. Electronic addresses: wur@uci.edu and shiming@tongji.edu.cn.

0.3 Pa, respectively. At first, 5.0 nm thick Pt layer was deposited at 600 °C and then 45.0 nm thick FePdPt layer was deposited at 520 °C from an FePdPt target. The deposition rates of the Pt and FePdPt layers were 0.1–0.2 nm/s. Finally, the sample was post-annealed in vacuum at 520 °C for 2 h. In experiments, the Pt(002) buffer layer was used to induce the expansion of the *a*- and *b*-axes of FePdPt and the contraction of the *c*-axis,[23,24] resulting in highly ordered $L1_0$ FePdPt alloy layer. The FePdPt target was formed by putting small pieces of Pd and Pt on an iron target. In order to keep the Fe atomic concentration unchanged, the area of Pt/Pd pieces was fixed for all samples. The Pt/Pd atomic concentration was controlled by changing the numbers of Pd and Pt pieces. The film thickness and microstructure were characterized by x-ray reflectivity (XRR) at small angles and x-ray diffraction (XRD) at large angles, respectively. The composition of alloy films was analyzed by energy dispersive X-ray (EDX) spectroscopy in combination with transmission electronic microscopy (TEM). Magnetization hysteresis loops were measured by physics properties measurement system (PPMS-9 T, Quantum Design, Inc.). The magneto-optical Kerr rotation angle θ_K and ellipticity ϵ_K spectra were measured by a home-made Kerr spectrometer in the visible region in the polar geometry.[25] The magnetic field is 10.0 kOe and angular resolution is 0.01°. The optical constants were measured by a home-made scanning ellipsometer at an incident angle of 70°.[26] Since the imaginary part of the refractive index k is in the region from 2.5 to 5.0 for $L1_0$ FePt and FePd films,[22] the influence of the buffer Pt layer can be neglected for 45 nm thick FePdPt layers, and the measured optical and MOKE properties are the intrinsic ones of the FePdPt layers. All measurements were made at room temperature.

FIRST-PRINCIPLES CALCULATIONS

In order to establish clear physical insights for the MOKE, we performed density functional theory (DFT) calculations with the Vienna *ab initio* simulation package (VASP),[27,28] at the level of the spin-polarized generalized-gradient approximation (GGA).[29] The interaction between valence electrons and ionic cores was described within the framework of the projector augmented wave (PAW) method.[30,31] The energy cutoff for the plane wave basis expansion was set to 350 eV. Four different compositions of the $L1_0$ FePdPt alloys were considered, with $x = 0.0$, 0.25, 0.5, and 1.0, using a $(2 \times 2 \times 2)$ supercell of 32 atoms. Since the lattice constants of $L1_0$ FePt and FePd are very close, we used the experimental lattice parameters of $L1_0$ FePt (a, $b = 3.86$ Å, $c = 3.71$ Å) for all cases. A $24 \times 24 \times 24$ k-grid mesh was used to sample the Brillouin zone.

The complex Kerr rotation depends on both the diagonal (σ_{xx}) and off-diagonal (σ_{xy}) elements of the conductivity tensor and can be expressed as[32]

$$\Phi_K = \theta_K + i\varepsilon_K = \frac{\sigma_{xy}}{\sigma_{xx}\sqrt{1 + i4\pi\sigma_{xx}/\omega}} = \frac{\sigma_{xy}}{D}, \quad (1)$$

with $D = \sigma_{xx}(1 + i4\pi\sigma_{xx}/\omega)^{1/2}$, θ_K and ε_K stand for the polar Kerr rotation and Kerr ellipticity, respectively. The optical conductivity tensor can be evaluated by means of the Kubo-Greewood linear response theory[33] and expressed as

$$\sigma_{\alpha\beta} = \frac{-ie^2}{m^2\hbar\Omega}\sum_k\sum_{mn}\frac{f_m - f_n}{\omega_{mn}}\frac{\Pi_{\alpha,nm}(\mathbf{k})\Pi_{\beta,mn}(\mathbf{k})}{\omega - \omega_{mn} + i\delta}. \quad (2)$$

Here, α and β are the indices of coordinates (x, y, or z), m and e are the mass and charge of an electron, $\hbar$ is the Plank constant, Ω is the volume of the unit cell, f_m is the Fermi function of electron occupancy, ω_{mn} is the energy difference between the nth and mth eigenvalues ($\hbar\omega_{mn} = \varepsilon_m - \varepsilon_n$), $\Pi_{\alpha,nm}(\mathbf{k}) = \langle\psi_n(\mathbf{k})|\Pi_\alpha|\psi_m(\mathbf{k})\rangle$ is the momentum matrix element between the nth and mth eigenstates, and δ is a broadening parameter which is chosen as 0.3 eV. In the framework of VASP-PAW approach, the momentum operator Π_α should be transformed to pseudo momentum operator $\tilde{\Pi}_\alpha$ as[30]

$$\tilde{\Pi}_\alpha = \Pi_\alpha + \sum_{i,j}|\tilde{p}_i\rangle(\langle\phi_i|\Pi_\alpha|\phi_j\rangle - \langle\tilde{\phi}_i|\Pi_\alpha|\tilde{\phi}_j\rangle)\langle\tilde{p}_j|. \quad (3)$$

Here, $\tilde{p}_i$ stands for the projector functions, ϕ_i and $\tilde{\phi}_i$ are all-electron and pseudo partial waves in the augmentation region, respectively.

RESULTS AND DISCUSSION

The XRR was measured for all substrate-MgO(002)/Pt (5 nm)/FePdPt (45 nm) samples. The film surface roughness is about 0.8 nm. Figure 1(a) shows the XRD of Pt/FePdPt bilayers with various Pt/Pd atomic concentrations. For all samples, the diffraction peak is near $2\theta = 24°$, indicating the long range structural ordering of the FePdPt layers. The peaks near $2\theta = 42$ and 49 (deg) result from the MgO(002) and FePdPt(002), respectively, the weak peak near $2\theta = 46.5°$ arises from Pt(002). Other peaks come from the MgO substrate. With the intensity ratio between (001) and (002) peaks, the chemical ordering degree S is calculated to be 0.8.[34,35] Note that the FePdPt (002) peak is close to the Pt(002) and MgO(002), so the XRD spectra in the region of $2\theta = 42°$–$50°$ need to be fitted by three Lorentz line peaks. Since the fabrication conditions of all samples are identical, their chemical ordering degree is expected to be about 0.8. In order to prove the epitaxial growth of FePdPt and Pt layers on the MgO(002) substrate, pole figures are given at $2\theta = 36°$ and 42° in Figs. 1(b) and 1(c). The image of a typical cross-sectional MgO(002)/Pt(002)/$L1_0$-FePd sample and the selected area diffraction pattern were also made. The results in Figs. 1(d) and 1(e) further confirm the epitaxial growth of FePdPt layer on MgO(002) substrate. As shown in Fig. 1(d), the sample is of ideal Pt/FePd interface. Figures 1(f) and 1(g) show the out-of-plane magnetization hysteresis loops of typical FePdPt samples. The samples are of in-plane anisotropy for small x and are perpendicularly magnetized for large x. For $x = 1$, the remnant ratio is equal to 1.0, and the out-of-plane saturation field is about 20 kOe, demonstrating strong perpendicular magnetic anisotropy. Other samples have the remnant ratio smaller than 1.0, indicating that the perpendicular magnetic anisotropy is smaller than the demagnetization energy. Therefore, the perpendicular

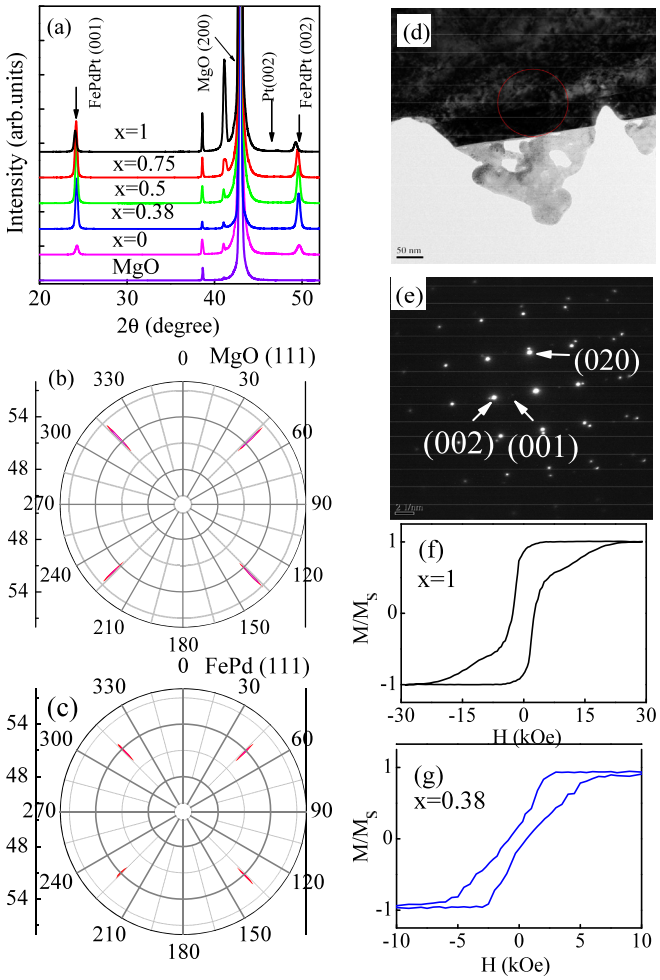

FIG. 1. XRD θ-2θ pattern of all samples (a), pole figures of MgO (002) substrate (b) and $L1_0$ FePd layer (c), and TEM cross sectional image (d), and selected area diffraction pattern (e), of a MgO(002)/Pt(002)/FePd(001) sample, and out-of-plane hysteresis loops of samples with $x = 1$ (f) and 0.38 (g).

magnetic anisotropy gradually increases with the increasing Pt/Pd atomic concentration.[36]

In polar MOKE measurements, all ternary alloy films except for $x = 1$ are saturated under the maximal magnetic field of 10 kOe in the polar geometry, whereas the $x = 1$ sample cannot be saturated. As well known, since the θ_K and ε_K for a specific sample are both proportional to the magnetization,[1] the saturation θ_K and ε_K can be obtained by the following equation $\Phi_K = \Phi_K(H_0) \times m_s/m(H_0)$, where m_s and $m(H_0)$ are the saturation magnetic moment and that of the out-of-plane minor hysteresis loop with the maximal magnetic field $H_0 = 10$ kOe, respectively. Figures 2(a) and 2(b) show the θ_K and ε_K spectra of typical FePdPt samples. A negative peak and a dip appear in the photon energy regions of 1.5 eV–2.0 eV and 2.5–3.5 eV, respectively. It is interesting that the θ_K peak and dip are gradually shifted towards higher energies with increasing x. In particular, the peak magnitude increases from 0.2° to 0.61° for x changing from 0 to 1.0. The θ_K peaks of $L1_0$ FePt and FePd films are enhanced, in comparison with those (0.18° and 0.41°) of disordered FePd and FePt alloys.[37,38] At the same time, the ε_K has a negative peak in the 1.7–2.6 eV region and a dip in 3.5–4.0 eV region. The position of the ε_K peak is located at

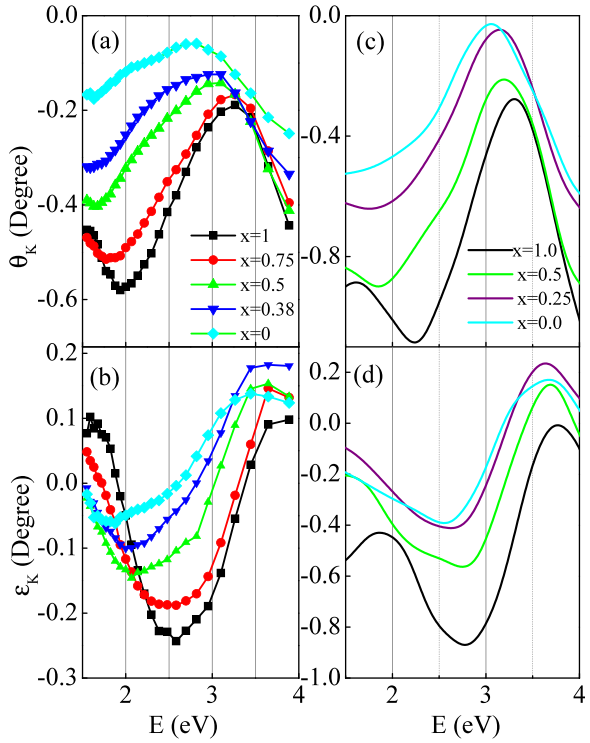

FIG. 2. Measured (a), (b) and calculated (c), (d) θ_K (a), (c) and ε_K (b), (d) spectra of typical samples in the visible region. The inset numbers in (a) and (c) refer to the Pt/Pd atomic concentration.

the energy for the sharp variation of θ_K. For the present $L1_0$ FePd and FePt films, the θ_K and ε_K spectra are close to the results provided by Lairson and Clemens[2] and their magnitudes are slightly smaller than the observed values by Cebollada and Armelles *et al.*,[6,21,22] possibly due to the less perfect chemical ordering degree ($S < 1$).[3]

For comparison, the DFT calculated Kerr rotation θ_K and ellipticity ε_K spectra are plotted in Figs. 2(c) and 2(d), respectively. Clearly, the theoretical spectra nicely follow the trend of the measured ones, although the peaks of θ_K and ε_K spectra shift upwards by about 0.3 eV and their magnitudes are about twice of the experimental values due to the assumption of perfect chemical ordering. These results demonstrate the validity of our method and parameters for the determination of the MOKE spectra of FePdPt alloys and serve as the foundation for the electronic analyses below.

To better understand the mechanism of the changes of the θ_K and ε_K spectra in Fig. 2, optical constants of MgO(002)/Pt(002)/$L1_0$ FePdPt samples were measured in the visible region. With the following relationship $\varepsilon_{xx} = \varepsilon_{xx1} + i\varepsilon_{xx2} = 1 + i4\pi\sigma_{xx}/\omega$ and $\varepsilon_{xx1} = n^2 - k^2$ and $\varepsilon_{xx2} = 2nk$, the real and imaginary parts of the diagonal element σ_{xx} are obtained. Figures 3(a) and 3(b) show that the real part σ_{xx1} slightly increases with decreasing energy, and the imaginary part σ_{xx2} exhibits a broad weak peak. The results of $L1_0$ FePt and FePd films are similar to those reported by Armelles *et al.*[22] More importantly, since neither σ_{xx1} nor σ_{xx2} changes much with x, the term $1/D$ in Eq. (1) is almost independent of the Pt/Pd atomic concentration and thus the evolution of the measured MOKE cannot be attributed to changes of the optical constants.

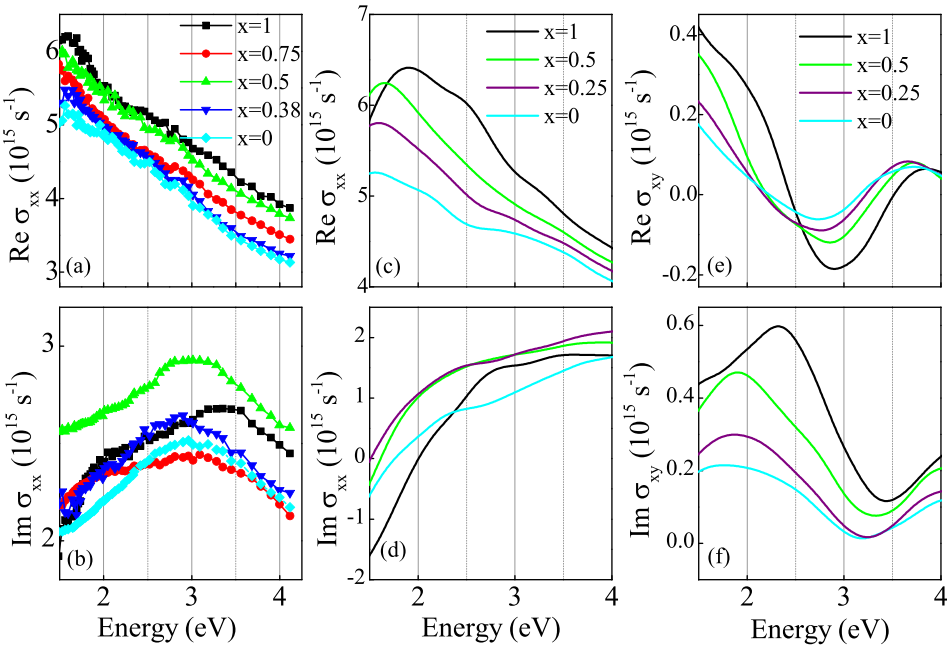

FIG. 3. Measured (a), (b) and calculated (c), (d) real (a), (c) and imaginary (b), (d) diagonal element σ_{xx} of the conductivity tensor of typical samples. In (e) and (f) are shown the calculated real and imaginary off-diagonal elements σ_{xy}, respectively.

The calculated diagonal σ_{xx} and off-diagonal σ_{xy} components of the conductivity tensor from DFT calculations are plotted in Figs. 3(c)–3(f). The trend of monotonic decrease of the real part of σ_{xx} from 2.0 to 4.0 eV for all cases agrees very well with the experimental measurements. Nevertheless, the broad peaks between 3.0 and 3.5 eV in the measured imaginary part of σ_{xx} are not captured in our calculations using the perfectly ordered model. Both the real and imaginary parts of σ_{xx} change slowly, so they contribute little to the shapes of the θ_K and ε_K spectra, unlike the observed results in (Ga, Mn)As.[17] On the contrary, the real and imaginary parts of σ_{xy} vary rapidly and show distinct features around the peaks in the θ_K and ε_K spectra. Therefore, the shapes of the θ_K and ε_K spectra are mainly determined by the anomalous Hall conductivity σ_{xy}. On the other hand, the magnitude of σ_{xy} decreases as the concentration of Pd increases, resulting in the decrease of the amplitude of the θ_K and ε_K peaks. This is understandable because the anomalous Hall conductivity σ_{xy} derives from the SOC interactions and the magnitudes of the σ_{xy} are proportional to the SOC strength, according to the second order pertubation theory.

Now, we identify the electronic origin of the anomalous Hall conductivity σ_{xy}, by splitting contributions from different spin channels to σ_{xx} and σ_{xy} of FePt and FePd, as shown in Fig. 4. In both cases, the σ_{xx} and σ_{xy} from the majority spin channel are almost constant, while those from the minority spin channel have similar shapes to the total σ_{xx} and σ_{xy} displayed in Fig. 3. Then, we calculated the element resolved θ_K of FePt and FePd by selectively switching off the SOC of either Fe or Pt(Pd).[39] It can be seen from Fig. 5 that the contributions from Fe are negligible for both cases. Furthermore, Pt has much larger contribution to θ_K than Pd, because of its stronger SOC strength. This explains the reason why the magnitude of the peak of the θ_K spectrum around 2.0 eV decreases with increasing Pd concentration.

The peaks of the θ_K and ε_K spectra are related to the transition of electrons from occupied bands to unoccupied bands, as denoted in Eqs. (2) and (3). To reveal the corresponding states for the transition, we analyzed the projected density of states (PDOS) of Pt-5*d* and Pd-4*d* orbitals in FePt and FePd. Since the *p* orbitals typically form featureless PDOS curve in a broad energy range, we perceive that all spectroscopic features only depend on the distribution of *d*-states. As shown in Fig. 6, the majority spin states of both Pt-5*d* and Pd-4*d* orbitals are almost fully occupied. Moreover, the PDOS curves of the Pt-5*d* and Pd-4*d* orbitals in the minority spin part are similar, except that the energy separation between the occupied and unoccupied states of Pt is larger than that of Pd. For example, the peak A of Pt-$d_{x^2-y^2}$ in FePt is at -2.3 eV whereas the corresponding peak B of Pd-$d_{x^2-y^2}$ in FePd is at -2.1 eV. For other samples with both Pt and Pd, this peak locates between A and B, as shown in the inset in Fig. 6(a) for $x = 0.5$. We find that the transition from A or B to the $p_{x/y}$ orbitals above the E_F in the minority spin channel contributes the most to the peak of the

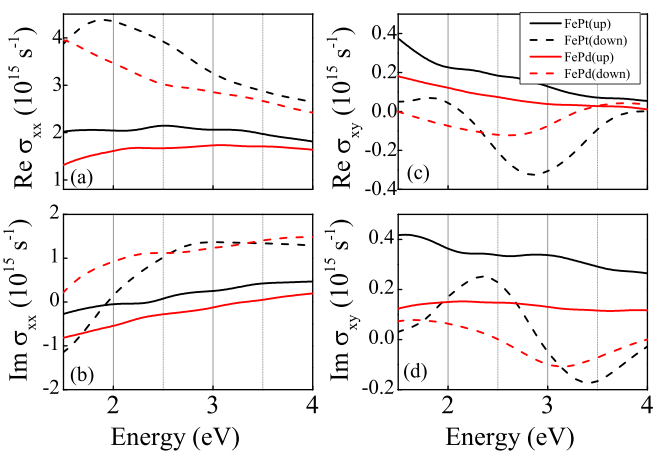

FIG. 4. The spin resolved spectra of real (a) and imaginary (b) σ_{xx} and real (c) and imaginary (d) σ_{xy} for $L1_0$ FePt and FePd.

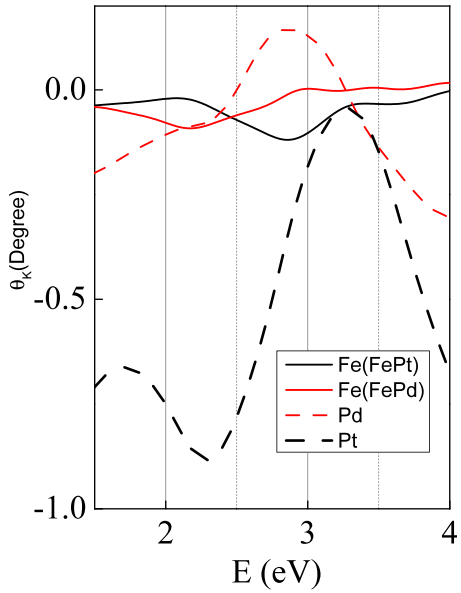

FIG. 5. The element resolved Kerr rotation of $L1_0$ FePt and FePd.

θ_K around 2.0 eV. Meanwhile, the transition from states of $d_{xz/yz}$ orbitals near −2.0 eV to the p_z orbital above the E_F also has a sizable contribution. The energy shift of the peak A to B during the substitution of Pt by Pd gives rise to the shift of the peaks of the θ_K spectrum within 1.6–2.2 eV and the ε_K spectrum within 2.6–2.8 eV.

It is significant to address the dependence of the MOKE on the SOC strength because the MOKE of magnetic materials arises from the interplay of SOC and exchange splitting. As shown in Fig. 7, the magnitude of the θ_K peak and the SOC strength ξ both increase with increasing x. Here, the SOC strength of the Pt/Pd site was taken from elsewhere.[36,40] The MOKE has been analyzed to mainly come from the

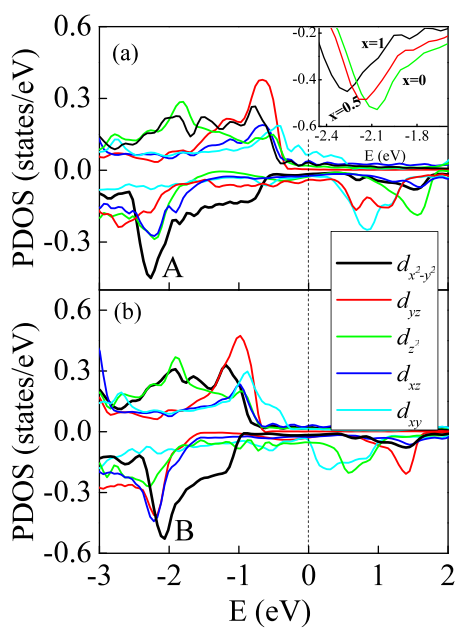

FIG. 6. The PDOS of all components of the d orbital of (a) Pt in $L1_0$ FePt and (b) Pd in $L1_0$ FePd. The inset in (a) shows the peaks of $d_{\downarrow,x^2-y^2}$ orbital of the Pt/Pd sites in $L1_0$ FePdPt with $x = 0$, 0.5, and 1.0.

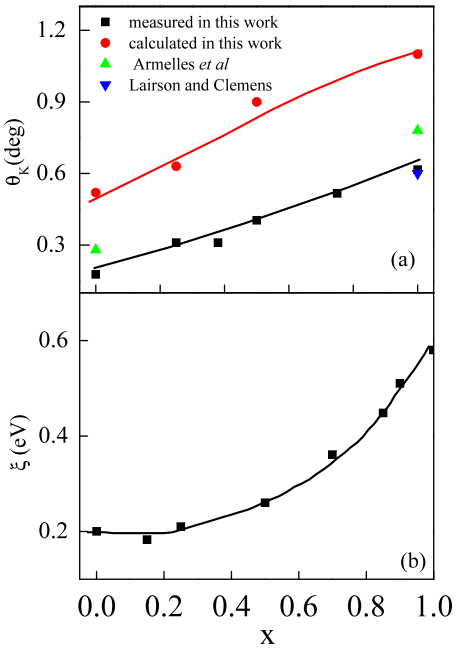

FIG. 7. The values of calculated and measured θ_K peaks (a) and the SOC strength (b) versus x. The data (solid ∇ and Δ) in (a) are taken from Ref. 2 and Refs. 21 and 22. The data of the SOC strength in (b) are taken from Refs. 36 and 40.

transition between $d_{\downarrow,x^2-y^2}$ and $p_{\downarrow,x/y}$ bands of the Pt/Pd atoms as discussed above. When the Pd atoms are replaced by heavier Pt one, the effective ξ in the alloy increases,[5] leading to redistribution among different components ($m = \pm 2, \pm 1$, and 0), and hence to large MOKE. The variations of both calculated and measured θ_K peak values with the SOC strength are found to deviate from the linear dependence.[15] When the SOC strength is tuned by changing the Pt/Pd concentration, the energy for both the maximal PDOS of $d_{\downarrow,x^2-y^2}$ and the θ_K peak shifts. Since the diagonal element of the conductivity tensor also slowly changes with energy, as shown in Figs. 3 and 4, the θ_K peak magnitude should also be modified due to the effect of optical constants, in addition to the effect of SOC strength. This results in the nonlinear dependence of the θ_K peak magnitude on the SOC strength. The SOC tuning effects have also been demonstrated on perpendicular magnetic anisotropy, anomalous Hall effect, and magnetic damping in $L1_0$ ordered alloys.[36,40]

CONCLUSION

To establish microscopic insight for the MOKE, we have fabricated epitaxial $L1_0$ FePdPt alloy films on MgO(002) substrates and studied their MOKE properties in the visible region. The magnitudes and positions of θ_K and ε_K peaks in the regions of 1.5–2.0 eV and 1.7–2.6 eV show strong dependence on the Pt/Pd atomic concentration, due to the tuning in the band width and the SOC strength. DFT calculations indicate that the MOKE spectroscopic feature mainly depends on the behavior of the off-diagonal element of the conductivity tensor or, furthermore, on optical transitions among the spin-down bands. The enhancement of θ_K magnitude for large x is assigned to the stronger SOC effect of the Pt atoms, but in a nonlinear way because of the scaling

factor of σ_{xx}. The $d_{\downarrow,x^2-y^2}$ bands of Pt and Pd atoms play the key role in determining the amplitude and energy position of the peaks and dips of θ_K and ε_K curves.

ACKNOWLEDGMENTS

This work was supported by the National Science Foundation of China Grant Nos. 11374227, 51331004, 51171129, and 51201114, the State Key Project of Fundamental Research Grant No. 2009CB929201, Shanghai Nanotechnology Program Center (No. 0252nm004), Shanghai Municipal Science and Technology Committee (Nos. 13XD1403700 and 13520722700), DOE-BES Grant No. DE-FG02-05ER46237 (J.H., M.C., and R.W.), and the National Science Council of Taiwan Grants (G.Y.G.). J.H., M.C., and R.W. also thank NERSC for computing time.

[1]P. N. Argyres, Phys. Rev. **97**, 334 (1955).
[2]B. M. Lairson and B. M. Clemens, Appl. Phys. Lett. **63**, 1438 (1993).
[3]S. Mitani, K. Takanashi, M. Sano, H. Fujimori, A. Osawa, and H. Nakajima, J. Magn. Magn. Mater. **148**, 163 (1995).
[4]Z. Q. Qiu and S. D. Bader, Rev. Sci. Instrum. **71**, 1243 (2000).
[5]T. Sugimoto, T. Katayama, Y. Suzuki, T. Koide, T. Sidara, M. Yuri, A. Itoh, and K. Kawanishi, Phys. Rev. B **48**, 16432 (1993).
[6]A. Cebollada, D. Weller, J. Sticht, G. R. Harp, R. F. C. Farrow, R. F. Marks, R. Savoy, and J. C. Scott, Phys. Rev. B **50**, 3419 (1994).
[7]I. Osterloh, P. M. Oppeneer, J. Sticht, and J. Kübler, J. Phys.: Condens. Matter **6**, 285 (1994).
[8]G. Y. Guo and H. Ebert, Phys. Rev. B **51**, 12633 (1995).
[9]Ya. Perlov, H. Ebert, A. N. Yaresko, V. N. Antonov, and D. Weller, Solid State Commun. **105**, 273 (1998).
[10]M. Yamaguchi, T. Kusakabe, K. Kyuno, and S. Asano, Physica B **270**, 17 (1999).
[11]H. Kanazawa, E. Ahmad, G. Lauhoff, and T. Suzuki, IEEE Trans. Magn. **37**, 1274 (2001).
[12]M. Kharoubi, A. Haroun, and M. Alouani, Comput. Mater. Sci. **73**, 24 (2013).
[13]D. Weller, H. Brandle, and C. Chappert, J. Magn. Magn. Mater. **121**, 461 (1993).
[14]H. Ebert, G. Y. Guo, and G. Schütz, IEEE Trans. Magn. **31**, 3301 (1995).
[15]H. Ebert, H. Freyer, A. Vernes, and G. Y. Guo, Phys. Rev. B **53**, 7721 (1996).
[16]M. Amft and P. M. Oppeneer, J. Phys.: Condens. Matter **19**, 315216 (2007).
[17]A. Stroppa, S. Picozzi, A. Continenza, M. Y. Kim, and A. J. Freeman, Phys. Rev. B **77**, 035208 (2008).
[18]M. Kumara, T. Nautiyal, and S. Auluck, J. Alloys Compd. **486**, 60 (2009).
[19]D. Sangalli, A. Marini, and A. Debernardi, Phys. Rev. B **86**, 125139 (2012).
[20]S. Yamamoto, M. Taguchi, M. Fujisawa, R. Hobara, S. Yamamoto, K. Yaji, T. Nakamura, K. Fujikawa, R. Yukawa, T. Togashi, M. Yabashi, M. Tsunoda, S. Shin, and I. Matsuda, Phys. Rev. B **89**, 064423 (2014).
[21]G. Armelles, D. Weller, B. Rellinghaus, P. Caro, A. Cebollada, and F. Briones, J. Appl. Phys. **82**, 4449 (1997).
[22]G. Armelles, D. Weller, B. Rellinghaus, R. F. C. Farrow, M. F. Toney, P. Caro, A. Cebollada, and M. I. Alonso, IEEE Trans. Magn. **33**, 3220 (1997).
[23]J.-U. Thiele, L. Folks, M. F. Toney, and D. K. Weller, J. Appl. Phys. **84**, 5686 (1998).
[24]A. C. Sun, J. H. Sun, P. C. Kuo, and H. L. Huang, Thin Solid Films **516**, 1155 (2008).
[25]L. Y. Chen, S. M. Zhou, Y. X. Zheng, Y. H. Qian, C. H. Shang, and Y. J. Wang, Opt. Eng. **36**, 3188 (1997).
[26]L. Y. Chen, X. W. Feng, Y. Su, H. Z. Ma, and Y. H. Qian, Appl. Opt. **33**, 1299 (1994).
[27]G. Kresse and J. Fürthmuller, Comput. Mater. Sci. **6**, 15 (1996).
[28]G. Kresse and J. Fürthmuller, Phys. Rev. B **54**, 11169 (1996).
[29]J. P. Perdew, K. Burke, and M. Ernzerhof, Phys. Rev. Lett. **77**, 3865 (1996).
[30]P. E. Blöchl, Phys. Rev. B **50**, 17953 (1994).
[31]G. Kresse and D. Joubert, Phys. Rev. B **59**, 1758 (1999).
[32]P. M. Oppeneer, T. Maurer, J. Sticht, and J. Kübler, Phys. Rev. B **45**, 10924 (1992).
[33]R. Kubo, J. Phys. Soc. Jpn. **12**, 570 (1957).
[34]P. S. Rudman and B. L. Avebrach, Acta Metall. **5**, 65 (1957).
[35]W. Roberts, Acta Metall. **2**, 597 (1954).
[36]P. He, X. Ma, J. W. Zhang, H. B. Zhao, G. Lupke, Z. Shi, and S. M. Zhou, Phys. Rev. Lett. **110**, 077203 (2013).
[37]K. H. J. Buschow, P. G. van Engen, and R. Jongebreur, J. Magn. Magn. Mater. **38**, 1 (1983).
[38]W. Reim, H. Brändle, D. Weller, and J. Schoenes, J. Magn. Magn. Mater. **93**, 220 (1991).
[39]G. Y. Guo and H. Ebert, J. Magn. Magn. Mater. **156**, 173 (1996).
[40]P. He, L. Ma, Z. Shi, G. Y. Guo, J. G. Zheng, Y. Xin, and S. M. Zhou, Phys. Rev. Lett. **109**, 066402 (2012).